

● *Original Contribution*

MYOCARDIAL ELASTOGRAPHY—A FEASIBILITY STUDY IN VIVO

ELISA E. KONOFAGOU,* JAN D'HOOGHE[†] and JONATHAN OPHIR[‡]

*Focused Ultrasound Laboratory Department of Radiology—MRI research, Brigham and Women's Hospital, Harvard Medical School, Boston, MA, USA; [†]Medical Image Computing, Department of Electrical Engineering, Cardiology and Physics, Catholic University Leuven, Leuven, Belgium; and [‡]Ultrasonics Laboratory, Department of Radiology, University of Texas Medical School Houston, Houston, TX, USA

(Received 29 August 2001; in final form 16 January 2002)

Abstract—Early detection of cardiovascular diseases has been a very active research area in the medical imaging field. Assessment of the local and global mechanical functions is one of the major goals of accurate diagnosis. In this study, we investigated the feasibility of elastography for estimation and imaging of the local cardiac muscle displacement and strain in a human heart *in vivo*. In its noninvasive applications, elastography has been typically used to determine local tissue strain through the use of externally applied compression. For our study, we utilized the cardiac muscle motion during a cardiac cycle as the mechanical stimulus, and acquired successive radiofrequency (RF) data frames of the septal and posterior walls over a few cardiac cycles in parasternal and apical views, respectively. High-quality ciné-loop elastograms were obtained due to high frame rates and the resulting low decorrelation noise. Furthermore, the strain contrast was higher in the parasternal case, when only the posterior wall was imaged, and strain estimation was more robust in the apical view. High repeatability of the results was observed through elastographic measurements over several cardiac cycles. Finally, an M-mode version of elastography was used to follow part of the interventricular septum or the posterior wall over the course of two cardiac cycles. Not only do these preliminary results show that elastography is feasible in cardiac applications *in vivo*, but also that it can provide new information regarding cardiac motion and mechanical function. Future prospects include assessment of the role of elastography in detection of ischemia and infarction. (E-mail: elisak@bwh.harvard.edu) © 2002 World Federation for Ultrasound in Medicine & Biology.

Key Words: Apex, Apical, Base, Cardiac, Compression, Contractility, Displacement, Elastogram, Elastography, M-mode, Myocardium, Parasternal, Strain, Tension, Ultrasound.

INTRODUCTION

Detection of cardiac dysfunction through assessment of the mechanical properties of the heart muscle has been a long-term goal in diagnostic cardiology. Ischemia and infarction can successfully be determined through characterization of the regional cardiac function. As a result, in a recent special issue of *Physics in Medicine and Biology* (Vol. 45(6), 2000) on tissue motion estimation and elasticity imaging, the majority of magnetic resonance imaging (MRI) techniques reported in that issue, such as cardiac tagging (Declercq et al. 2000; Ozturk and McVeigh 2000) and harmonic phase (HARP) (Osman and Prince 2000), dealt with cardiac applications. Despite the fact that several ultrasound (US)-based motion-

estimation techniques were also reported in the same issue, none were in conjunction with echocardiography.

Echocardiography, however, still remains the predominant imaging modality in diagnostic cardiology due to its real-time feedback, high temporal resolution and a multitude of complementary methods that can be used for a complete and accurate diagnosis. The two main areas of investigation are motion-estimation techniques and tissue-characterization methods. Motion-estimation techniques include Doppler myocardial imaging (DMI) (McDicken et al. 1992; Sutherland et al. 1994; Zamorano et al. 1997) and strain rate imaging (SRI) (Heimdahl et al. 1998), which use Doppler techniques to obtain regional velocity estimates and velocity gradients (or, strain rates) of the myocardium, respectively. The field of tissue characterization, a complement to the motion-estimation techniques, measures acoustic parameters such as attenuation (O'Donnell et al. 1979; Verdonk et al. 1996), speed of sound (Auld 1990) and integrated backscatter

Address correspondence to: Elisa E. Konofagou, Ph.D., Department of Radiology - MRI research, Brigham and Women's Hospital, Harvard Medical School, LMRC #013, 221 Longwood Ave., Boston, MA 02115 USA. E-mail: elisak@bwh.harvard.edu

(IB) (Sigelmann and Reid 1973; Wear et al. 1989; Miller et al. 1985; Van der Steen et al. 1997; D'hooge et al. 2000) to determine such myocardial attributes as thickening and thinning (cyclic variation) (Madaras et al. 1983), and anisotropy (Hoffmeister et al. 1996). In fact, IB measurements and strain estimates have been qualitatively shown to be equivalent (D'hooge 1999). A brief, but thorough, overview of the tissue characterization methods is given in Miller et al. (1998).

The aforementioned motion-estimation techniques are mainly Doppler-based methods (*i.e.*, they employ autocorrelation techniques to track the phase shift caused by the cardiac motion). There have been several disadvantages associated with phase-shift-based methods discussed in the literature (Bonnetfous and Pesqué 1986; Hein and O'Brien 1993; Jensen 1996). The main ones are the limitation to small bandwidth signals (*i.e.*, low axial resolution) (Bonnetfous and Pesqué 1986; de Jong et al. 1990; Hein and O'Brien 1993; Jensen 1996), aliasing (occurring at half the center frequency), the increase in ambiguity of the estimation with the center frequency (Bonnetfous and Pesqué 1986) and attenuation effects (Brands et al. 1997). It is of no surprise that the DMI methods also inherit the shortcomings associated with the phase shift (or autocorrelation) methods (Heimdal 1999). Time-shift-based methods, such as cross-correlation and sum-of-absolute-difference (SAD) estimators, have been repeatedly shown to overcome the main limitations of low resolution and aliasing associated with phase-shift methods and, at the same time providing higher precision (Bonnetfous and Pesqué 1986; Bohs and Trahey 1991; Hein and O'Brien 1993; Hoeks et al. 1993; Jensen 1996). Despite the fact that cardiac applications were of interest since the beginning of the development of motion-estimation techniques (de Jong et al. 1990; Adler et al. 1990), time-shift based techniques in cardiac applications *in vivo* have only been reported on M-mode data (Kanai et al. 1997, 1999) or envelope-detected data (Meunier et al. 1987, 1988; Meunier 1989).

Elastography (Ophir et al. 1991, 1999) is a technique that calculates local tissue strain through cross-correlation of radio-frequency (RF) segments for the estimation of the time shift resulting from a small deformation. The resulting image of the local tissue strain is called an *elastogram*. Based on the principle of palpation, elastography was initially designed for the detection of stiffer masses (*i.e.*, tumors) inside healthy tissue and has been shown to have successful results in muscle (Kallel et al. 1998), prostate (Kallel et al. 1999) and breast (Céspedes et al. 1993; Garra et al. 1997) in *in vitro* and *in vivo* applications (Ophir et al. 1999). Because assessment of the myocardial mechanical parameters has proven to be a crucial step in the detection of cardiac abnormalities, elastography should have a significant im-

pact in this field by measuring the mechanical response of the cardiac muscle at the various steps of the cardiac cycle (Konofagou et al. 2000). In this case, the cardiac stimulus is used instead of the externally applied compression, in a similar way to the intravascular elastography using the arterial contraction to measure strain inside the vessel (de Korte et al. 1997), but noninvasively.

For this study, we concentrated on a healthy volunteer case to determine the feasibility and robustness of the application of elastography on the cardiac muscle. The two examples of left ventricular muscle considered were the interventricular septum in an apical view, which is a muscular wall that separates the left from the right ventricle, and the posterior wall in a parasternal view. Below, we start by providing the methods used for the generation of cardiac elastograms and proceed to show and discuss the motion and deformation results.

METHODS

The septal and posterior walls of a 28-year-old healthy male volunteer were scanned in apical four-chamber (A4C) and parasternal long-axis (LAX) views, respectively, using a Vingmed System FiVe (GE Vingmed, Horten, Norway) and a 2.5-MHz phased array. The apical view was particularly chosen in this feasibility study, because the data set could be acquired in such a way that the septum moves along each A-line (*i.e.*, minimizing the lateral motion). In-phase and quadrature (IQ) data were acquired and transferred to a workstation for off-line analysis and converted to RF. The sampling frequency was equal to 20 MHz and the depths and widths scanned were equal to 90 mm and 10 mm, respectively.

Incremental (*i.e.*, between successive frames) axial displacement and axial strain estimates were obtained using a cross-correlation method in which temporally successive RF segments were applied (Ophir et al. 1991; Céspedes et al. 1995; Konofagou and Ophir 1998), using a window equal to 2 mm and a window overlap of 80% to assure high elastographic resolution (Alam and Ophir 2000). The frame rate was varied between 60 and 710 Hz with the subsequent observed trade-off in spatial resolution. To ensure the high temporal resolution used in this study (120 Hz) and, thereby, low decorrelation between frames, 8 (10° angle) and 10 (15° angle) RF A-lines per frame were acquired in the parasternal and apical cases, respectively. Due to the low decorrelation noise and low lateral sampling, no recorrelation methods were employed (Konofagou and Ophir 1998). Sonographic data of the entire cardiac view were not acquired simultaneously, but M-mode data are provided for comparison with the elastographic results. Finally, a 5 × 5 median

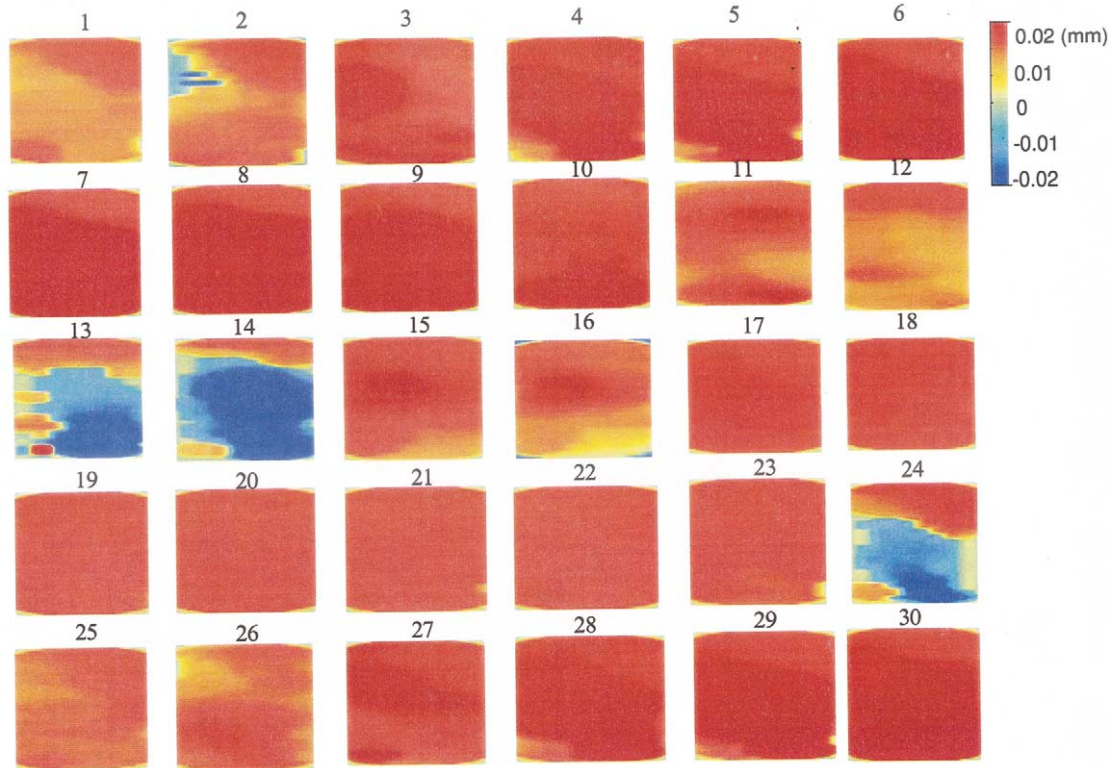


Fig. 1. Displacement images within the septal muscle in the A4C view: 1–24: first cycle; 25–30: first part of second cycle. The apex is found toward the top of the images (Fig. 2, at 0-mm depth) and the base toward the bottom (Fig. 2, at 90-mm depth).

filter was applied to all images shown here to compensate for the low lateral sampling.

RESULTS

The transducer was located at the top of all apical images and at the bottom of all parasternal images shown in this paper. Furthermore, the reader should note that the general conventions of elastography are kept (*i.e.*, positive (negative) displacement denotes motion toward (away from) the transducer and positive (negative) strain denotes compression, tension). All displacement images and conventional elastograms are of size 10 (or 8) mm across and 90 mm depth, but are shown in a square format to facilitate viewing. A series of displacement images from an apical view is first shown in Fig. 1 at regular intervals during the cardiac cycle. Frames 1–24 represent 0–97% of the first cycle. Frame 25 represents the onset of the second cycle and, thus, frames 26–30 correspond to frames 2–6 of the first cycle.

During one cardiac cycle, the ventricular wall contracts during systole and ejection, and relaxes during diastole and filling. During systole, the interventricular septum shrinks towards the apex as it contracts. During

diastole, it relaxes back toward the base. Frames 6 and 7 show highest positive displacement (*i.e.*, motion of the septal muscle towards the transducer, at the apex). They correspond, thus, to the ejection phase of the left ventricle, when the basal septum moves from the base towards the apex (Fig. 2). Frame 14 in Fig. 1 shows highest negative displacement of the muscle close to the base, signifying the muscle moving away from the apex (or transducer). This occurs at the early or fast-filling phase of the left ventricle, when the septum gradually relaxes toward the base. Frames 17–23 correspond to diastasis (accounting for ~40% of the cardiac cycle in this case) and frame 25 correlates well with the displacement mapping of frame 1, signifying the beginning of the next cardiac cycle.

In Fig. 2, an M-mode sonogram, an M-mode version of Fig. 1, and a plot of the local displacement variation over two cardiac cycles allows further identification of several cardiac events. During ejection (E) the base (at a depth of 90 mm) moves closer (positive displacement rising) to the apex (at a depth of 0 mm), then starts to slow down approaching isovolumic relaxation (IVR), when the displacement follows an initial

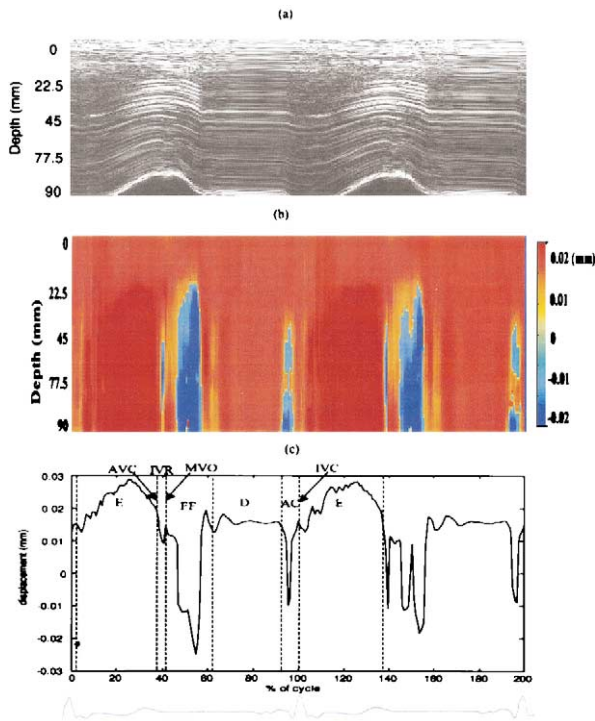


Fig. 2. (a) M-mode sonogram of the interventricular septum in the apical view. (b) M-mode images of an axial line segment through the displacement image (20% off the right end of the images in Fig. 1; same scale used). Depths of 0-mm and 90-mm are closer to the apex and base, respectively. (c) Temporal profile of displacement at 45-mm depth, showing the cardiac events over one cardiac cycle. E = ejection, AVC = aortic valve closure, IVR = isovolumic relaxation, MVO = mitral valve opening, FF = fast filling, D = diastasis, AC = atrial contraction. The EKG is merely used here as reference.

drop. During fast-filling (FF), the muscle stretches from apex to base and the displacement progressively decreases (or muscle moves towards the base). It then levels off during diastasis (D) to a constant displacement level, denoting rigid motion (orange area in M-mode), and momentarily drops to negative levels during late (or, atrial) filling (AC), when the muscle stretches toward the base again. Note that, during diastasis, a rigid motion of the muscle (i.e., motion without deformation) occurs (the displacement is not zero, but stays constant). In the second cycle, the displacement follows an almost identical pattern.

The conventional elastograms (Fig. 3) and the M-mode elastogram (Fig. 4) show the same trend. During ejection, the septum experiences compressive (positive) strain (frames 6–7) and, during fast filling, the muscle undergoes tensile (negative) strain (frames 13–14). The noisy appearance of elastograms 13 and 14 is due to blood echoes entering the field-of-view (FOV) during filling (see also Fig. 1/frames 13 and 14). The upper part

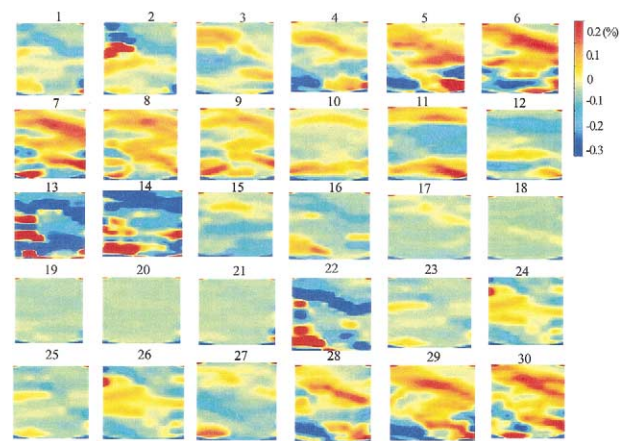


Fig. 3. Elastograms in the A4C view, 1–24: first cycle; 25–30: first part of second cycle. The apex is at the top of the images (Fig. 2, at 0-mm depth) and the base at the bottom (Fig. 2, at 90-mm depth).

of the interventricular septum (i.e., the one closest to the apex) appears to undergo the highest compressive strain during ejection. During diastasis, the strain is practically zero (frames 17–23), confirming the lack of deformation also seen with the displacement tracings. Frames 25–30 again show the second cardiac cycle elastograms, closely following the strain distribution and variation of their equivalent frames in the first cycle (i.e., frames 1–6). In Fig. 4, the septal area undergoing the highest compression is shown to have moved closest to the apex at the end of the ejection, which is expected because the base

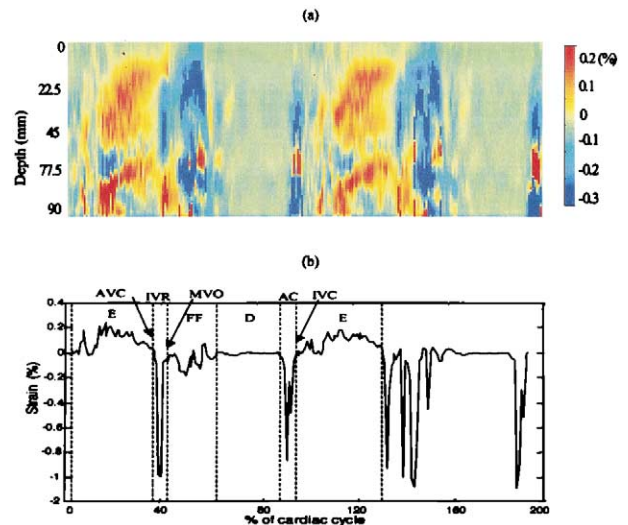


Fig. 4. (a) M-mode images of an axial line segment through the elastogram (20% off the right end of the images in Fig. 3; same scale used). (b) Temporal strain profile at 45-mm depth, showing the cardiac events over one cardiac cycle. Labeling same as in Fig. 2.

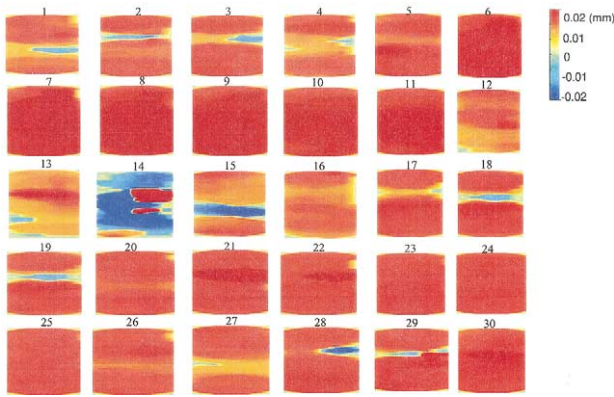


Fig. 5. Displacement images in the LAX view. 1–24: first cycle; 25–30: first part of second cycle. The epicardium is at the top of the images (Fig. 4, at 0-mm depth) and the ventricular cavity at the bottom (Fig. 4, at 90-mm depth).

has moved closest to the apex at this point, shrinking down the septum. The temporal strain profile of Fig. 4 also shows the compressive (E), tensile (FF and AC) and virtually no strain (D) of the septum over two cardiac

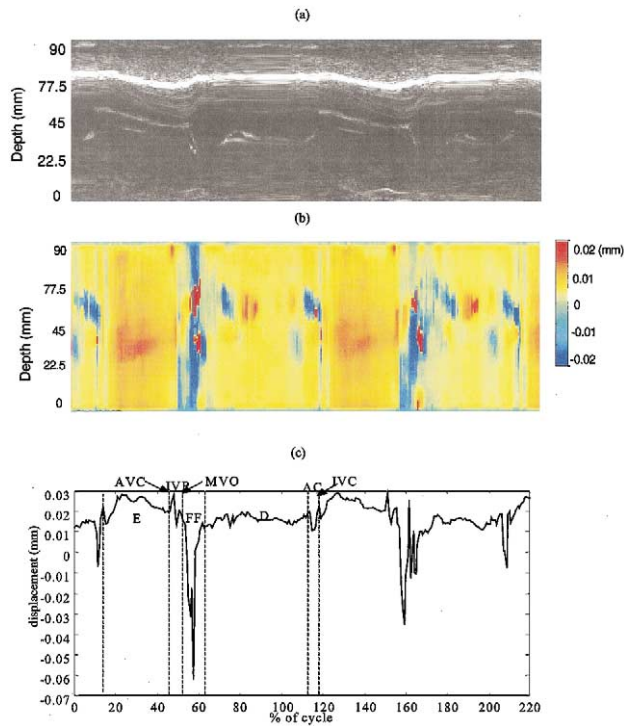


Fig. 6. (a) M-mode sonogram of the structure in the parasternal view (the hyperechoic interface denotes the epicardium). (b) M-mode displacement image following an axial line segment through the series of displacement images of Fig. 5 (20% off the right end of the images in Fig. 5; same scale used). (c) Temporal displacement profile at 55-mm depth, showing the cardiac events over one cardiac cycle. The scale is the same as that in Fig. 5.

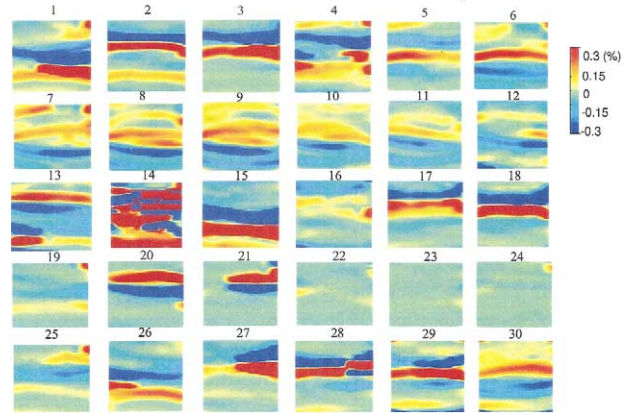


Fig. 7. Elastograms in the LAX view. 1–24: first cycle; 25–30: first part of second cycle.

cycles. The M-mode results of Figs. 2 and 4 compare well with those obtained with DMI techniques, showing the displacement and strain gradient from base to apex (that stays practically fixed during a cycle) (McDicken *et al.* 1992).

Figures 5, 6, 7 and 8 are the exact equivalents of Figs. 1, 2, 3 and 4 in the parasternal long-axis view case. In this case, a higher displacement (Fig. 5) and strain (Fig. 7) contrast was observed around a distinct horizontal structure (particularly seen in frames 1–5 and 15–18) of the posterior wall. In Fig. 6, the M-mode displacement image and temporal profile also allow for the identification of several events of posterior wall contraction and

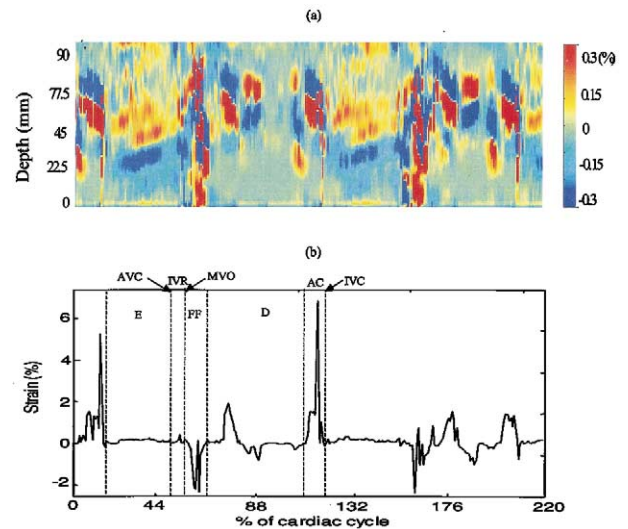


Fig. 8. (a) M-mode images of an axial line segment through the elastogram (20% off the right end of the images in Fig. 7; same scale used). (b) Temporal strain profile at 55-mm depth, showing the cardiac events over one cardiac cycle.

relaxation. The most interesting results, however, were obtained with the elastograms. In the series of elastograms, throughout virtually all nondiastolic frames, the strain throughout the muscle is highly non-uniform. In fact, the elastograms depict two distinct regions: one close to the endocardium (top) undergoing compression in virtually all frames and one close to the epicardium (bottom) undergoing tension. Also, a pair of compressive and tensile strain regions with changing polarity (e.g. in frames 2–3 and 20) appears around the posterior wall and the muscle seems to be split into two areas that are experiencing opposite strains. In Fig. 7, from frame 1 to frame 5, tensile strain occurs close to the endocardium, forcing the muscle to stretch away from the ventricular cavity, preparing for the ejection phase, at the onset of which it reverses “strain polarity” (frame 6), and the muscle wall closest to the endocardium is now undergoing compressive strain. From frame 6 to frame 13, the tension (endocardium)/compression (epicardium) polarity is preserved and, after the end of the ejection phase (frame 14), the polarity is reversed to compression (endocardium)/tension (epicardium) denoting the onset of the fast-filling phase (frame 16). The muscle seems then to adjust itself, after reversing the strain polarity yet again (frames 20–21) to reach diastasis (frames 22–24). The same polarity behavior is then observed in the second cycle (frames 25–30). The M-mode elastogram of Fig. 8 also shows the polarity change inside the posterior wall during a cycle and over different cardiac cycles, as noted. Note that the position of the strain polarity (inverted or not) follows the cyclical change of the position of the pericardium, as shown in the M-mode sonogram of Fig. 6.

DISCUSSION

The basic function of the cardiac muscle is to deform (*i.e.*, contract and relax) in order to pump blood throughout the body continuously. Therefore, by definition, it constitutes an ideal organ to be studied with elastography, a method designed to image tissues and to detect abnormalities during or following a deformation. The general consensus used to be that the three-dimensional (3-D) complicated motion of the left ventricular wall during a cardiac cycle and the high computational intensity, usually and wrongly associated with elastography, would prevent it from playing an important role in assessing the mechanical properties of the cardiac muscle *in vivo*. Given the importance of early detection of cardiac abnormalities for an efficient combat of cardiovascular disease, several US-based methods have been developed to measure tissue characterization and motion-estimation parameters that may be related to the mechanical properties of the cardiac muscle. The mo-

tion-estimation techniques reported until now typically apply Doppler methods to estimate velocity and, thus, inherit many of the disadvantages associated with Doppler. MRI-based methods, such as cardiac tagging, have also been repeatedly shown to estimate the eigenvalues and eigenvectors of the strain tensor, but at the cost of spatial resolution (*i.e.*, limited by tag spacing) and low temporal resolution.

In this study, we showed how incremental axial (*i.e.*, along the ultrasonic beam) displacement and strain could be estimated and imaged within the interventricular septum (apical view) and posterior wall (parasternal view). A healthy patient was used so that the motion pattern is familiar and repeatability of motion and deformation results over several cardiac cycles could be verified. Both the incremental (*i.e.*, occurring between successive sonographic frames) displacement and strain estimates were obtained at high signal-to-noise ratio (SNR) throughout several cardiac cycles. This is because they vary within the dynamic range that has been shown to be optimal for elastography (Varghese and Ophir 1997; Konofagou et al. 2000). The displacement images show the distribution of the motion of different structures within the interventricular septum and the posterior wall in the apical and parasternal views, respectively. The M-mode displacement image allows us to follow a particular motion distribution with time and identify gradients with time, and is highly correlated to the motion indicated by the M-mode sonograms. These M-mode results verify findings reported with SRI (Heimdal 1999). SRI measures the total strain occurring in the muscle during a cardiac cycle through integration of the strain rate curve.

In elastography, unlike SRI, strain is obtained directly from the displacement estimates without compromising the spatial resolution and without being limited by the temporal resolution, as is the case when integrating the strain-rate curve (Heimdal 1999). However, the strain measured here is incremental (*i.e.*, between successive frames) while SRI typically measures the cumulative strain. In addition, strain is mapped across the cardiac structures studied and the distribution of contraction and relaxation could be temporally monitored (Figs. 3 and 7). The conventional elastogram sequence in both views discussed shows that the deformation throughout the cardiac cycle is not uniform, neither within the interventricular septum nor within the posterior wall. In fact, in the latter case, the strain contrast was shown to be much higher than in the former. Several explanations could be given for this finding, all of them relating to the distinct myocardial fiber orientation between the two views. First, the interventricular septum is known to be more uniform than the posterior wall that encompasses the epicardium and endocardium. Most importantly,

Streeter and Hanna (1973) showed the angular dependence of the Young's modulus of the left-ventricular wall that exhibited a progressive transmural shift in fiber orientation from approximately $+60^\circ$ at the endocardial surface to -60° at the epicardial surface. Second, the myofibers constituting the interventricular septum are parallel to the ultrasonic beam in the apical view, and the myofibers of the posterior wall are perpendicular to the ultrasonic beam in the parasternal view (Recchia *et al.* 1993). Therefore, the posterior wall is expected to present higher strain contrast than the more uniform interventricular septum. Indeed, in the parasternal case the strain distribution was found to be much more inhomogeneous than in the apical case with two distinct regions across the myocardium undergoing opposite deformations. In addition, in the parasternal view, a strain polarity around a horizontal structure was shown to be reversed over several cardiac events (Figs. 7 and 8) and followed the motion of the pericardium (Fig. 6). This effect may be indicative of the normal function of the muscle but, given the novelty of these results, no conclusions can be drawn yet. Still, this polarity may constitute a signature of healthy myocardium. The M-mode elastograms allowed the localization of the high compressive or tensile strain over a particular segment, both spatially and temporally. The comparison of M-mode elastograms in the apical view (Fig. 4) and parasternal view (Fig. 8) clearly indicates the more uniform strain distribution across the interventricular septum as opposed to the continuous polarity inversion and high strain contrast across the posterior wall. Finally, the region of adjacent opposite strains could be due to the strongly reflecting pericardium that could bias the strain estimate one way or the other.

The strain estimation achieved with elastography can provide important insight into several muscle properties. Its spatial distribution relates to both the stiffness and structure of the fibers. Its variation with time could indicate abnormalities when lack of contractility is observed. The dependence of strain magnitude on fiber orientation relative to the ultrasonic beam constitutes a goal of future investigations. Furthermore, the low lateral sampling that assured the high image quality prevented the estimation of 2-D strain. However, it has been shown that 2-D strain estimation is feasible (Meunier *et al.* 1988, Konofagou and Ophir 1998; D'hooge *et al.* 2002). In addition, reports in the literature have indicated that the use of envelope-detected data with elastography may be sufficient for highlighting several cardiac events (Meunier *et al.* 1987, 1988; Meunier 1989; Konofagou *et al.* 2001). Future investigations will involve the increase in PRF without compromising lateral sampling to obtain multidimensional displacement and strain mapping using RF and/or envelope-detected data. Clinical applications

in the detection of cardiac disease constitutes the long-term goal.

CONCLUSION

Elastography was shown to be feasible in cardiac applications *in vivo* to provide important new information on the mechanical and structural properties of the ventricular wall, both spatially and temporally, at high resolution and precision. Future investigations should determine the role of elastography in the diagnosis of ischemia and infarction.

Acknowledgement—This work was supported in part by National Cancer Institute Program Project Grant PO1-CA 64597 to the University of Texas.

REFERENCES

- Adler RS, Rubin JM, Bland PH, Carson PL. Quantitative tissue motion analysis of digitized M-mode images: Gestational differences in fetal lung. *Ultrasound Med Biol* 1990;16:561–569.
- Alam SK, Ophir J. Elastographic resolution: An experimental study. *IEEE Trans Ultrason Ferroelec Freq Control* 2000;47(1):304–308.
- Auld BA. *Acoustic fields and waves in solids*. Vol. 1. 2nd ed. Malabar, FL: Robert E. Krieger Publishing, 1990.
- Bohs LN, Trahey GE. A novel method for angle independent ultrasonic imaging of blood flow and tissue motion. *IEEE Trans Biomed Eng* 1991;38:280–286.
- Bonnefous O, Pesqué P. Time domain formulation of pulse-Doppler ultrasound and blood velocity estimation by cross-correlation. *Ultrasound Imaging* 1986;8:73–85.
- Brands PJ, Hoeks APG, Ledoux IAF, Reneman RS. A radio-frequency domain complex cross-correlation to estimate blood flow velocity and tissue motion by mean of ultrasound. *Ultrasound Med Biol* 1997;23:911–920.
- Céspedes I, Huang Y, Ophir J, Spratt S. Methods for estimation of subsample time delays of digitized echo signals. *Ultrasound Imaging* 1995;17:142–171.
- Céspedes I, Ophir J, Ponnekanti H, Maklad N. Elastography: Elasticity imaging using ultrasound with application to muscle and breast *in vivo*. *Ultrasound Imaging* 1993;15:73–88.
- D'hooge J. Interaction of ultrasonic waves and tissues: Modeling, simulations and applications. Ph.D. thesis, Katholieke Universiteit, Leuven, Belgium, 1999.
- D'hooge J, Bijmens B, Jamal F, Pislaru C, Thoen J, Suetens P, Van de Werf F, Angermann C, Rademakers F, Herregods MC, Sutherland GR. High frame rate myocardial integrated backscatter. Does this change our understanding of this acoustic parameter? *Eur J Echocardi* 2000;1(1):32–41.
- D'hooge J, Konofagou EE, Jamal F, Heimdal A, Barrios L, Bijmens B, Thoen J, Van de Werf F, Sutherland G, Suetens P. Two-dimensional strain rate measurement of the human heart *in vivo*. *IEEE Trans Ultrason Ferroelec Freq Control* 2002;49:281–286.
- de Jong PGM, Hoeks APG, Reneman RS. Determination of tissue motion velocity by correlation interpolation of pulsed ultrasonic echo signals. *Ultrasound Imaging* 1990;12:84–98.
- de Korte CL, Céspedes EI, van der Steen AFW, Lancellotti CT. Intravascular elasticity imaging using ultrasound: Feasibility studies in phantoms. *Ultrasound Med Biol* 1997;23:735–746.
- Declercq J, Denney TS, Ozturk C, O'Dell W, McVeigh ER. Left ventricular motion reconstruction from planar tagged MR images: A comparison. *Phys Med Biol* 2000;45:1611–1632.
- Garra BS, Céspedes EI, Ophir J, Spratt RS, Zurbier RA, Magnant CM, Pennanen MF. Elastography of breast lesions: Initial clinical results. *Radiology* 1997;202:79–96.
- Heimdal A. Doppler based ultrasound imaging methods for noninva-

- sive of tissue viability. Ph.D. thesis, Norwegian University of Science and Technology, 1999.
- Heimdal A, Stoylen A, Torp H, Skjaerpe T. Real time strain rate imaging of the left ventricle by ultrasound. *J Am Soc Ech* 1998; 11(11):1013–1019.
- Hein IA, O'Brien WD. Current time-domain methods for assessing tissue motion by analysis from reflected ultrasound echoes—A review. *IEEE Trans Ultrason Ferroelec Freq Control* 1993;40:84–102.
- Hoeks APG, Arts TG, Brands PJ, and Renaman RS. Comparison of the performance of the rf crosscorrelation and Doppler autocorrelation technique to estimate the mean velocity of simulated ultrasound signals. *Ultrasound Med Biol* 1993;19:727–740.
- Hoffmeister BK, Handley SM, Wickline SA, Miller JG. Ultrasonic determination of the anisotropy of Young's modulus of fixed tendon and fixed myocardium. *J Acoustic Soc Am* 1996;97:3171–3176.
- Jensen JA. Estimation of blood velocities using ultrasound. Cambridge, UK: Cambridge University Press, 1996.
- Kallel F, Ophir J, Magee K, Krouskop T. Elastographic imaging of low contrast elastic modulus distributions in tissue. *Ultrasound Med Biol* 1998;24:409–425.
- Kallel F, Price R, Konofagou EE, Ophir J. Elastographic imaging of the dog prostate *in vitro*. *Ultrason Imaging* 1999;21(3):201–215.
- Kanai H, Hasegawa H, Cubachi N, Koiwa Y, Tanaka M. Non-invasive evaluation of local myocardial thickening and its color-coded imaging. *IEEE-UFFC* 1997;44:752–768.
- Kanai H, Koiwa Y, Zhang J. Real-time measurements of local myocardial motion and arterial wall thickening. *IEEE-UFFC* 1999;46:1229–1241.
- Konofagou EE, Ophir J. A new elastographic method for estimation and imaging of lateral strains, corrected axial strains and Poisson's ratios in tissues. *Ultrasound Med Biol* 1998;24(8):1183–1199.
- Konofagou EE, D'hooge J, Ophir J. Cardiac elastography — A feasibility study. *IEEE Proceedings of Symposium in Ultrasonics, Ferroelectrics and Frequency Control*, San Juan, Puerto Rico, 2000; 1273–1276.
- Konofagou EE, Harrigan T, Solomon S. Assessment of regional myocardial strain using cardiac elastography: Distinguishing infarcted from non-infarcted myocardium. *IEEE Proceedings of Symposium in Ultrasonics, Ferroelectrics and Frequency Control*, Atlanta, GA, 2001;1589–1602.
- McDicken WM, Sutherland GR, Moran CM, Gordon LN. Colour Doppler velocity imaging of the myocardium. *Ultrasound Med Biol* 1992;18:651–654.
- Madaras EI, Barzilai B, Perez JE, Sobel BE, Miller JG. Changes in myocardial backscatter throughout the cardiac cycle. *Ultrason Imaging* 1983;5:229–239.
- Meunier J. Analyse dynamique des textures d'échographies bidimensionnelles du myocarde. Ph.D. dissertation. Ecole Polytechnique Montreal, 1989.
- Meunier J, Bertrand M, Mailloux G. A model for dynamic texture analysis in two-dimensional echocardiograms of the myocardium. *SPIE* 1987;768:193–200.
- Meunier J, Bertrand M, Mailloux G, Peticlerc R. A model for dynamic texture analysis in two-dimensional echocardiograms of the myocardium. *SPIE* 1988;914(1):20–29.
- Miller JG, Perez JE, Sobel BE. Ultrasonic characterization of myocardium. *Progress Cardiovascu Dis* 1985;28:85–110.
- Miller JG, Perez JE, Wickline SA, Baldwin SL, et al. Backscatter imaging. *IEEE-UFFC Symposium*, Sendai, Japan, 1998.
- O'Donnell M, Mimbs JW, Miller JG. The relationship between collagen and ultrasonic attenuation in myocardial tissue. *J Acoust Soc Am* 1979;65:512–517.
- Ophir J, Alam SK, Garra B, Kallel F, Konofagou EE, Krouskop T, Varghese T. Elastography: ultrasonic estimation and imaging of the elastic properties of tissues. *Proc Inst Mech Eng* 1999;213:203–233.
- Ophir J, Céspedes I, Ponnekanti H, Yazdi Y, Li X. Elastography: A quantitative method for imaging the elasticity of biological tissues. *Ultrason Imaging* 1991;13:111–134.
- Osman NF, Prince JL. Visualizing myocardial function using HARP MRI. *Phys Med Biol* 2000;45:1665–1682.
- Ozturk C, McVeigh ER. Four-dimensional B-spline based motion analysis of tagged MR images: Introduction and in vivo validation. *Phys Med Biol* 2000;45:1683–1703.
- Recchia D, Miller JG, Wickline SA. Quantification of ultrasonic anisotropy in normal myocardium with lateral gain compensation of two-dimensional integrated backscatter images. *Ultrasound Med Biol* 1993;19:497–505.
- Sigelmann RA, Reid JM. Analysis and measurement of ultrasonic backscattering from an ensemble of scatterers excited by sine-wave bursts. *J Acoust Soc Am* 1973;53:1351–1355.
- Streeter DD, Hanna WT. Engineering mechanics for successive states in canine left ventricular myocardium. II. Fiber angle and sarcomere length. *Circ Res* 1973;33:656–664.
- Sutherland GR, Stewart MJ, Groundstroem WE, Moran CM, Fleming A, Guell-Peris FJ, Riemersma RA, Fenn LN, Fox KAA, McDicken WN. Color Doppler myocardial imaging: A new technique for the assessment of myocardial function. *J Am Soc Echocardiog* 1994; 7:441–458.
- van der Steen AFW, Rijsterborgh H, Lancee CT, Mastik F, Krams R, Verdouw PD, Roelandt JRTC, Bom N. Influence of data processing on cyclic variation of integrated backscatter and wall thickness in stunned porcine myocardium. *Ultrasound Med Biol* 1997;23(3): 405–414.
- Varghese T, Ophir J. A theoretical framework for performance characterization of elastography: The Strain Filter. *IEEE Trans Ultrason Ferroelec Freq Control* 1997;44:164–172.
- Verdonk ED, Hoffmeister BK, Wickline SA, Miller JG. Anisotropy of the slope of ultrasonic attenuation in formalin fixed human myocardium. *J Acoust Soc Am* 1996;99:3837–3843.
- Wear KA, Milunski MR, Wickline SA, Perez JA, Sobel BE, Miller JG. Differentiation between acutely ischemic myocardium and zones of completed infarction in dogs on the basis of frequency-dependent backscatter. *J Acoust Soc Am* 1989;85:2634–2641.
- Zamorano J, Wallbridge DR, Ge J, Drozd J, Nesser J, Erbel R. Non-invasive assessment of cardiac physiology by tissue Doppler echocardiography. *Eur Heart J* 1997;18(2):330–339.